


# Improved fuzzy neural network control for the clamping force of Camellia fruit picking manipulator

Ziyan Fan , Lijun Li\*, Kai Liao, Zicheng Gao, Yuhang Li, and Hao Xie

College of Mechanical and Electrical Engineering, Central South University of Forestry and Technology, Changsha 410000, China

Received: 19 May 2022 / Received in final form: 22 April 2023 / Accepted: 9 July 2023

**Abstract.** During the operation of the vibrating mechanism, the push-shaking camellia fruit picking manipulator needs to ensure a constant force output of the clamping hydraulic motor in order to make sure that the camellia fruit tree trunk wouldn't loosen or damage, which may affect its later growth, during the picking process. In this regard, this paper derived the state space model of the valve-controlled clamping hydraulic motor system of the push-shaking camellia fruit picking manipulator, and the fuzzy wavelet neural network (FWNN) was designed on the basis of the traditional incremental PID control principle and the parameters of the neural network were optimized by the improved grey wolf optimizer (GWO). And then, the control system was simulated with the MATLAB/Simulink software without and with external interference, and compared and analyzed it with traditional PID controller and fuzzy PID (FPID) controller. The results show that the traditional PID controller and the FPID control have slow response and poor robustness, while the improved fuzzy wavelet neural network PID (IFWNN PID) controller possesses the characteristics of fast response and strong robustness, which can well meet the requirement of the constant clamping force of hydraulic motors. Finally, the field clamping test was carried out on the picking manipulator. The results show that the manipulator controlled by the IFWNN PID controller shortens the clamping time by 20.0% and reduces the clamping damage by 13.6% compared with the PID controller, which is verified that the designed controller can meet the clamping operation requirements of the camellia fruit picking machine.

**Keywords:** Camellia fruit picking manipulator / clamping force PID control / fuzzy wavelet neural network / improved grey wolf optimization algorithm

## 1 Introduction

- The constant clamping force control of the electromechanical-hydraulic integrated manipulator requires not only to avoid too small clamping force to prevent clamping loose during vibration picking, but also to avoid excessive clamping force of the clamping jaws to avoid excessive damage to the trunk.
- The electro-hydraulic proportional directional valve and the electro-hydraulic proportional relief valve are used to control the pressure and flow of the hydraulic system of the clamping jaws at the same time. The relief valve is used to roughly adjust the clamping force, and the directional valve is used to finely adjust the clamping force.
- The learning algorithm of fuzzy wavelet neural network is optimized by using the improved gray wolf optimization algorithm, which improves the efficiency of the neural network.
- 

The field test verifies that manipulator controlled by the IWNNPID controller controls shorted the clamping jaw movement time in 20%, and reduced the clamping damage in 13.6%.

Camellia is an important oil crop in China, which has high edible and medicinal value [1]. Studies have shown that using camellia to make food can effectively lower blood pressure and avoid the occurrence of cardiovascular and cerebrovascular diseases. In addition, camellia is also widely used to make high-end cosmetics. According to the statistics of the State Forestry and Grassland Administration of China, the planting area of camellia in China has reached 45.34 billion square meters in 2020, with a total output value of \$17.97 billion, which has driven nearly 2 million people in rural areas to lift themselves out of poverty. However, manual picking is the current main picking method of camellia fruit, and with the development of China's economy, the labor cost is getting higher and higher with low picking efficiency, which has led to the fact that manual picking is gradually becoming a negative factor hindering the development of the camellia industry.

\* e-mail: [junlili1122@163.com](mailto:junlili1122@163.com)

At present, the research on mechanized picking of camellia fruit is in its infancy. The basic research directions are mainly divided into comb picking [2], vibration picking, rubber roller picking [3] and clamp picking [4]. Among them, vibration picking has become the current mainstream mechanized picking operation due to its high picking efficiency [5]. The vibrating camellia fruit picking machine mainly fixes and clamps the camellia fruit tree branches that need to be shaken by adjusting the moving clamping mechanism, and then vibrates by driving the picking actuator. When the exciting force generated by the vibration exceeds the binding force between the camellia fruit and the branch, the camellia fruit automatically falls off the branch which realizes mechanized picking [6]. It is critical to maintain the clamping force of the camellia tree in the vibration for the vibrating picking machine. If the clamping force is too small, the clamping jaws will loosen during vibration picking, which will cause the failure of the picking operation, while the clamping force is too large, the camellia branches will be seriously damaged, affecting the growth and future yield of the camellia tree. Therefore, it is of great significance to study the control of the clamping force of the camellia fruit picking manipulator.

At present, the classic control method in the control field is to use the PID controller to carry out closed-loop control of the force control system, that is, to realize the control of the system by adjusting the three links of proportional, differential and integral [7–10]. However, the traditional PID controller is difficult to achieve an ideal control effect for such a complex valve-controlled hydraulic motor system. According to the opinions of references [11–13], fuzzy control doesn't require precise mathematical models of the controlled object and has strong robustness [14–16]. According to references [17,18], fuzzy PID control has been widely used in the field of robot control in complex environments. Its control effect on PID controller depends on the richness of experts' experience in this area, because fuzzy control needs to rely on expert experience to compile control rules, which becomes a disadvantage of fuzzy PID controllers. Lou and the other researchers [19] took the lead in introducing fuzzy neural network PID control into the field of fluid control in 2012, and designed a gate flow control system. This controller has both advantages of PID controller and fuzzy neural network self-learning and processing quantitative data [20], and has better control accuracy and effect. Gong and Yang [21] began to introduce fuzzy neural network PID control into the field of hydraulic control, and designed an oil pump control system suitable for outdoor operations in complex mountainous areas. The controller proved to have good anti-interference ability and good adaptability. However, the electromechanical-hydraulic integrated robots in agricultural and forestry mainly use the hydraulic valve control system for its operation control, and the flow control system of the variable pump is less used due to its high cost. Therefore, this paper uses the fuzzy neural network to control the flow of the valve-controlled hydraulic motor system.

This paper firstly analyzed the clamping hydraulic system of camellia fruit picking manipulator, clarified its working principle, and established a mathematical model of the system on this basis. Then a FWNN PID controller

was designed combined with the basic principles of PID control, fuzzy control and wavelet neural networks. Finally, MATLAB/Simulink was used to simulate and analyze the control system under different working conditions, and field tests were carried out to verify the effectiveness of the control method.

## 2 The working principle and mathematical model of the picking manipulator

### 2.1 Introduction of the picking manipulator

Figure 1 shows the structure of the push-shaking camellia fruit picking manipulator, which consists of a clamping mechanism and a vibration picking mechanism. The clamping mechanism is composed of a clamping hydraulic motor 7, a bevel gear pair 9, a clamping spline screw 10, a clamping nut 11, clamping links 12 and clamping jaws 13. During clamping operation, the clamping hydraulic motor 7 drives the clamping spline screw 10 to rotate through the bevel gear pair 9, and drives the clamping nut 11 to rotate on the screw 10 to realize the clamping and loosening of the jaws. The vibration picking mechanism is composed of a vibration hydraulic motor 4, a vibration crank disk 6 and a vibration connecting link 7. The vibrating hydraulic motor 4 drives the vibrating crank disk 6 to generate eccentric rotation, and drives the vibrating connecting link 7 to generate reciprocating vibration during picking operation. The monocular camera 2 is installed at the front end of the picking manipulator to identify the camellia trunk to be clamped and picked.

### 2.2 Mathematical model of the clamping mechanism

#### 2.2.1 Mathematical model of clamping hydraulic motor

The flow continuity equation for the clamping hydraulic motor is:

$$Q_L = D \frac{d\theta}{dt} + K_{cm} P_L + \frac{V_m}{E} \frac{dP_L}{dt} \quad (1)$$

Where:

- $E$  — the elastic modulus of hydraulic oil;
- $K_{cm}$  — the hydraulic motor leakage coefficient;
- $P_L$  — the hydraulic motor inlet pressure;
- $Q_L$  — the hydraulic motor oil inlet flow;
- $D$  — the theoretical displacement of the hydraulic motor;
- $V_m$  — the volume of the hydraulic motor oil inlet chamber;
- $\theta$  — the rotation angle of the output shaft of the hydraulic motor.

The balance equation for the force on the clamping hydraulic motor shaft is:

$$\frac{DP_L}{2\pi} = J_t \frac{d^2\theta}{dt^2} + c_m \frac{d\theta}{dt} + G\theta \quad (2)$$

where:

- $J_t$  — the total moment of inertia of the hydraulic motor shaft;

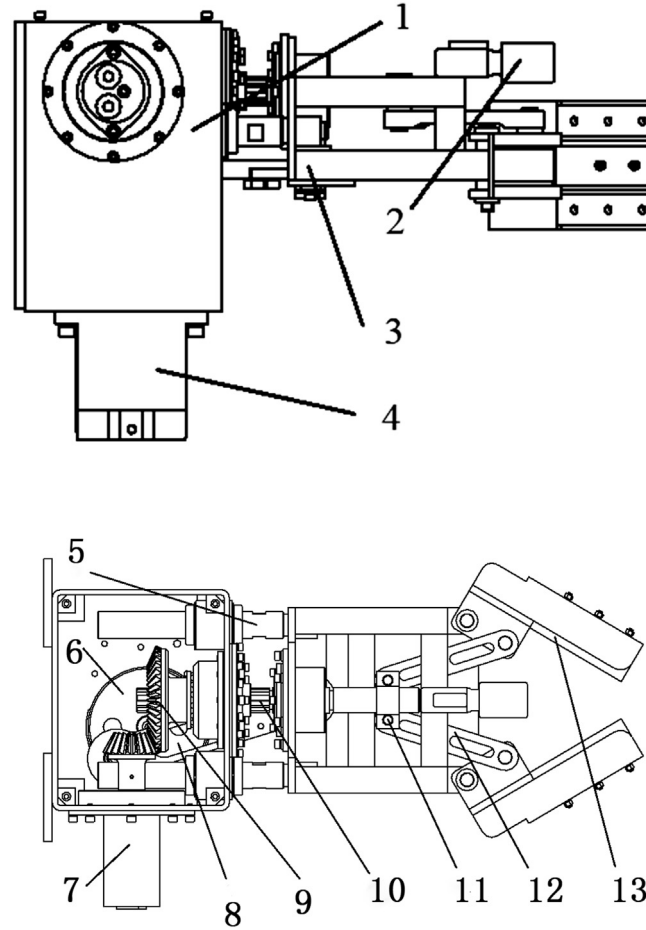


**Fig. 1.** Structure of picking manipulator: 1. Housing, 2. monocular camera, 3. vibrating head bracket, 4. vibrating hydraulic motor, 5. guide link, 6. vibrating crank disk, 7. clamping hydraulic motor, 8. vibrating connecting link, 9. clamping bevel gear pair, 10. clamping spline screw, 11. clamping nut, 12. clamping link, 13. clamping jaw.

$c_m$  — the viscous damping coefficient of the hydraulic motor and the load;

$G$  — the torsional spring stiffness of the load.

The output shaft torque of the hydraulic motor is:

$$T_0 = \frac{DP_L}{2\pi}. \quad (3)$$

### 2.2.2 Mathematical model of clamping mechanism

The driving torque  $T_1$  transmitted by the clamping hydraulic motor 7 to the spline screw 10 through the bevel gear pair 9 is:

$$T_1 = \eta_1 i T_0 \quad (4)$$

where:

$\eta_1$  — the transmission efficiency of the gear pair;

$i$  — the transmission ratio of the gear pair.

The transmission relationship between the spline screw 10 and the clamping nut 11 can be expressed as:

$$F_A = \frac{2\pi T_1 \eta_2}{L} \quad (5)$$

where:

$F_A$  — the thrust of the clamping nut 11;

$\eta_2$  — the transmission efficiency of the nut screw;

$L$  — the lead of the screw.

The mechanism movement relationship between 11, 12 and 13 can be simplified as a rocker-slider mechanism, of which the schematic diagram is shown in Figure 2.

The clamping links and the clamping jaws are taken as the force analysis objects, of which the gravity is ignored. The force analysis diagram is shown in Figure 3.

According to Figure 3, the equation of the output clamping force at the end of the clamping jaws is:

$$\begin{cases} F_A = 2F_B \cos \alpha \\ F_D d_{CD} - F_B d_{BC} = 0 \end{cases} \quad (6)$$

where:

$F_B$  — the thrust of the clamping links to the clamping jaw;

$F_C$  — the support reaction force of the manipulator;

$F_D$  — the reaction force of camellia trees to the clamping jaw;

$\alpha$  — the horizontal angle between the clamping links and the screw shaft;

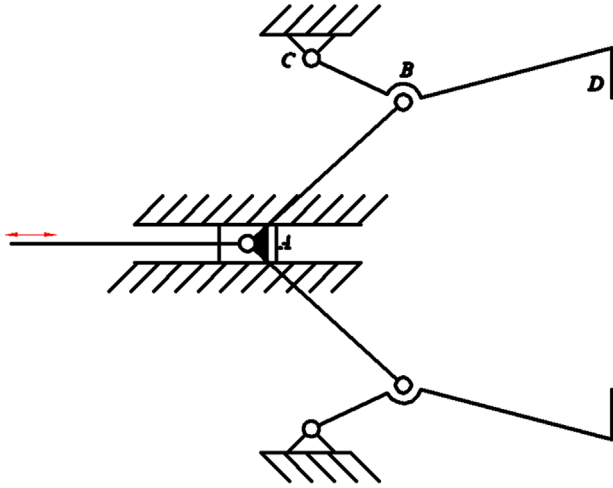


**Fig. 2.** Schematic diagram of the movement of the clamping mechanism.

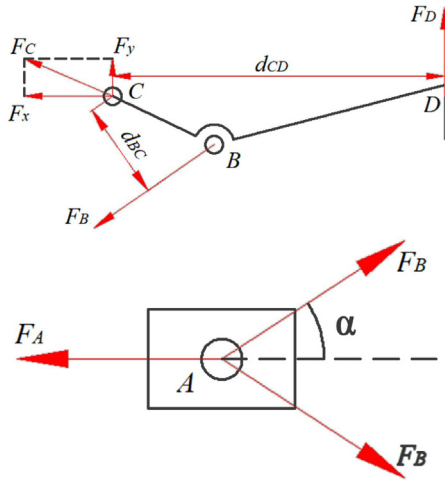


**Fig. 3.** Force analysis diagram of clamping jaws.

$d_{BC}$  — the vertical distance between the clamping jaw  $BC$ ;  
 $d_{CD}$  — the vertical distance between the clamping jaw  $CD$ .

Due to the symmetry of the clamping jaws, only half of it needs to be modeled and analyzed when exploring the kinematic relationship between its joint angle and the clamping nut displacement  $s$ . As shown in **Figure 4**, a plane rectangular coordinate system is established with the projection of point  $B_0$  on the horizontal axis of the spline screw when the jaws open and close at the maximum as the origin  $O$ . When the moving distance of the jaws in the horizontal direction is  $s$ , the kinematics relationship of each link of the clamping jaws is:

$$s = l_{AB} \cos \alpha + l_{BC}(1 - \cos \gamma) - \sqrt{l_{AB}^2 - e^2} \quad (7)$$

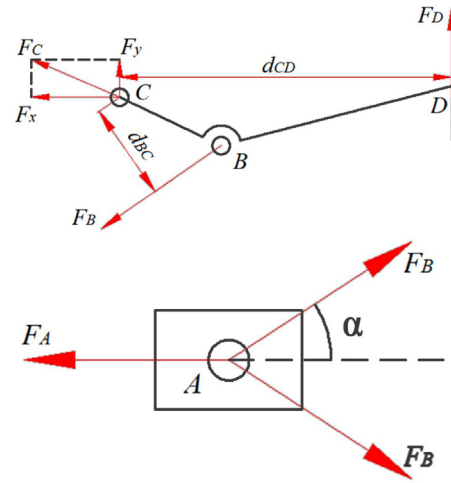


**Fig. 4.** Kinematic analysis diagram of clamping jaws.

where:

$l_{AB}$  — the projected length of the clamping link  $AB$  to the ground;

$l_{BC}$  — the projected length of the clamping jaw  $BC$  to the ground;

$\gamma$  — the rotation angle of the clamping jaw around  $C$ ;

$e$  — the vertical distance from  $C$  to the spline screw.

Then according to the plane geometric relationship:

$$\beta = \alpha + \gamma \quad (8)$$

$$l_{AB} \sin \alpha + l_{BC} \sin \gamma = e. \quad (9)$$

Then the relationship between the vertical distance  $d_{BC}$  between the jaws  $B$  &  $C$  and the links length clamping links  $l_{AB}$  is:

$$d_{BC} = l_{BC} \sin \beta. \quad (10)$$

The relationship between the moving distance  $s$  of the clamping jaws in the horizontal direction and the output shaft angle  $\theta$  of the hydraulic motor is:

$$s = \frac{L\theta}{2\pi i}. \quad (11)$$

The force transmission ratio between the output torque  $T_0$  of the hydraulic motor and the clamping force  $F_D$  is defined as:

$$\xi_0 = \frac{F_D}{T_0}. \quad (12)$$

Bring the above equations (4)–(11) into equation (12), and get:

$$\xi_0 = k_1 \theta + k_2. \quad (13)$$

In the formula:  $k_1$  and  $k_2$  are constants related to the jaw structure, transmission ratio and transmission efficiency.

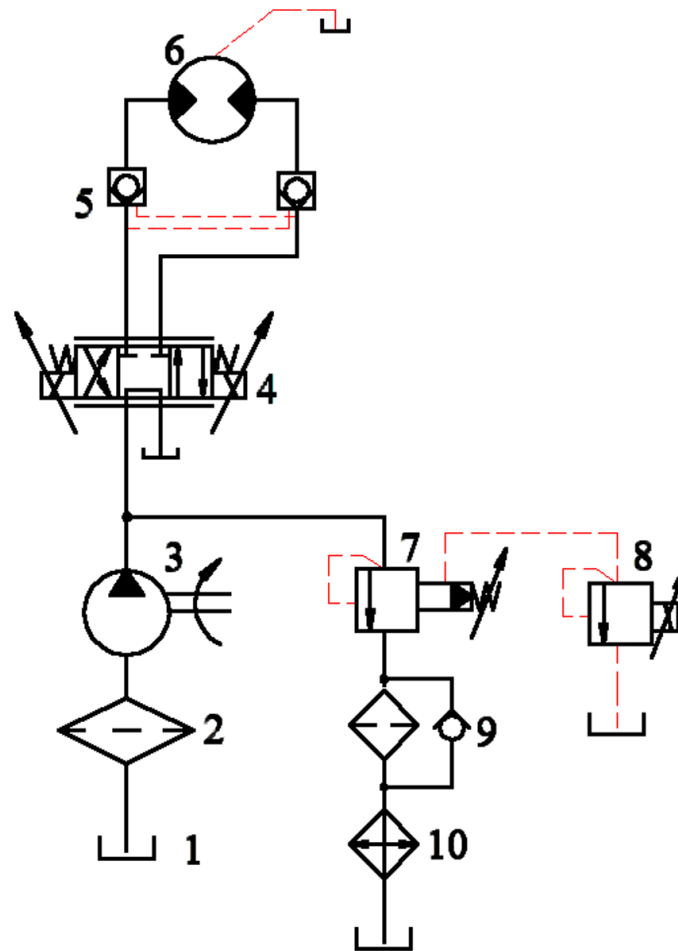


**Fig. 5.** Simplified hydraulic schematic of the clamping hydraulic motor: 1. tank, 2. pump oil filter, 3. Pump, 4. electro-hydraulic proportional direction valve, 5. bidirectional hydraulic lock, 6. clamping hydraulic motor, 7. pilot-operated relief valve, 8. electro-hydraulic proportional relief valve, 9. one-way oil filter, 10. cooler.

Equation (13) shows that there is a linear function relationship between the designed jaw force transmission ratio and the rotation angle  $\theta$  of the hydraulic motor. When the hydraulic motor rotation angle  $\theta$  reaches the maximum value, that is, the moving distance  $s$  of the clamping jaws in the horizontal direction just reaches the end of the clamping spline screw, the output clamping force of the clamping jaw reaches the maximum value at this time. It can be analyzed that the size of the clamping force  $F_D$  at the end of the clamping jaw can be controlled by controlling the output shaft angle  $\theta$  and the output pressure of the hydraulic motor combined with formula (3).

In summary, the output clamping force and the opening angle of the hydraulic manipulator can be achieved by controlling the pressure and flow rate of the hydraulic oil input to the clamping hydraulic motor.

### 2.2.3 Electro-hydraulic control scheme and mathematical modeling of components

According to the analysis above, the hydraulic principle diagram of the picking manipulator was designed as shown in Figure 5.

When the camellia tree clamping operation is realized, the right electromagnet of the reversing valve 4 is energized, the hydraulic pump 3 supplies oil to the clamping hydraulic motor 6, and the motor 6 rotates forwardly, so that the clamping jaws are closed to grip the camellia tree. Bidirectional hydraulic locks 5 are designed at both ends of the clamping hydraulic motor 7 to lock the oil circuit of the clamping hydraulic motor 6 in order to prevent the gripped camellia branches from loosening during the vibration picking process. After the vibration harvesting is completed, the left electromagnet of the valve 4 is energized, and the clamping hydraulic motor 6 is reversed, so that the clamping jaws can release the camellia tree.

According to the above analysis of equation (13), it can be seen that the control of the clamping force of the manipulator needs to ensure the constant rotation angle of the hydraulic motor and the pressure of the oil inlet. Therefore, an electro-hydraulic proportional direction valve 4 is designed to control the flow of the hydraulic motor, and an electro-hydraulic proportional relief valve 8 is installed on the pilot valve of the pilot-operated relief valve 7 to flexibly adjust the system pressure input to the hydraulic motor. The control system flexibly adjusts

the pressure of the relief valve 8 according to the data of the camellia trunk to be clamped measured by the vision system, and then controls the pressure of the hydraulic system to determine the maximum clamping force output by the clamping jaws. The control system controls the input current of the valve 4 and changes its valve opening, thereby realizing the control of the rotation angle and output torque of the clamping hydraulic motor, and realizing the stable and flexible gripping of the clamping jaws.

The following is the mathematical modeling process of electro-hydraulic proportional direction valve.

The displacement  $x_v$  of the electro-hydraulic proportional direction valve spool is proportional to the input current  $I$ , namely:

$$x_v = K_i I \quad (14)$$

where:

$K_i$  — the constant coefficient of proportionality.

Assuming that the oil supply pressure  $p_s$  is constant and the oil return pressure  $p_o$  is zero, the dynamic flow equation of the electro-hydraulic proportional direction valve is:

$$Q_L = C_{dv} W_v x_v \sqrt{\frac{2(p_{v1} - p_{v2})}{\rho}} \quad (15)$$

where:

$C_{dv}$  — the flow coefficient;

$W_v$  — the area gradient, that is, the width of the valve port in the circumferential direction;

$p_{v1}$  — the oil pressure of the oil inlet of the electro-hydraulic proportional direction valve;

$p_{v2}$  — the oil pressure at the outlet of the electro-hydraulic proportional direction valve;

$\rho$  — the hydraulic oil density.

By linearizing the above formula, the linearized flow increment equation of the electro-hydraulic proportional direction valve can be obtained as:

$$Q_L = K_q x_v - K_c P_L \quad (16)$$

where:

$$K_q = \frac{\partial Q_L}{\partial x_v} \text{ — the flow gain;}$$

$$K_c = \frac{\partial Q_L}{\partial (p_{v1} - p_{v2})} \text{ — the coefficient of flow pressure.}$$

In summary, The hydraulic motor output shaft rotation angle  $\theta$ , hydraulic motor output shaft speed  $d\theta/dt$ , and hydraulic motor oil inlet pressure  $P_L$  are selected as the state variables  $x_1, x_2, x_3$ , the current  $i$  is taken as the input variable, and the output angle  $\theta$  and torque  $T_0$  of the hydraulic motor are taken as the output variables combined with the above equations (1)~(3) and (14)~(16). The state space model of the system is constructed as follows:

$$\dot{x} = A_1 x + B_1 u y = C_1 x \quad (17)$$

where:

$$A_1 = \begin{bmatrix} 0 & 1 & 0 \\ -\frac{G}{J_t} & -\frac{c_m}{J_t} & \frac{D}{2\pi J_t} \\ 0 & -\frac{DE}{V_m} & -\frac{(K_c - K_{cm})E}{V_m} \end{bmatrix}$$

$$B_1 = \begin{bmatrix} 0 & 0 & \frac{k_q k_i E}{V_m} \end{bmatrix}^T$$

$$C_1 = \begin{bmatrix} 0 & 0 & \frac{D}{2\pi} \\ 1 & 0 & 0 \end{bmatrix}.$$

According to the above state equation, it can be seen that the opening and closing angle  $\theta$  of the gripper and the clamping force  $F_D$  would be controlled by adjusting the input current  $I$  of the electro-hydraulic proportional direction valve.

### 3 Design of fuzzy neural network PID controller

#### 3.1 Design of PID controller

The control law of incremental digital PID is as follows:

$$\begin{aligned} \Delta u(k) &= u(k) - u(k-1) \\ &= K_p [e(k) - e(k-1)] + K_I e(k) + K_D \left[ \begin{matrix} e(k) - 2e(k-1) \\ + e(k-2) \end{matrix} \right] \end{aligned}$$

In the formula:  $u(k)$  and  $u(k-1)$  are the  $k$ th and  $(k-1)$ th output values of the controller;  $K_p$  is the proportional coefficient;  $K_I$  is the integral coefficient;  $K_D$  is the differential coefficient;  $e(k)$ ,  $e(k-1)$  and  $e(k-2)$  are the  $k$ th,  $(k-1)$ th, and  $(k-2)$ th input error values.

It is difficult to achieve the optimal control effect, when the control system of the clamping hydraulic motor adopts PID controller to adjust the three parameters of proportional, integral and differential. Therefore, the fuzzy neural network is used to adaptively adjust these three parameters in PID. The input and output function relationship of the fuzzy neural network is shown in the following formula(18), and the control flow chart of the fuzzy neural network PID controller is presented in Figure 6.

$$\{ K_P = f_1(e, \cdot e) K_I = f_2(e, \cdot e) K_D = f_3(e, \cdot e) \quad (18)$$

#### 3.2 Design of fuzzy wavelet neural network

According to the above, this paper needs to design a fuzzy neural network to adjust the three parameters of the PID system, and the FWN has the dual advantages of wavelet neural network and fuzzy control system which concludes fast speed, strong learning ability and robustness that can well meet the working conditions of the Camellia fruit picking manipulator. Therefore, this paper chooses the

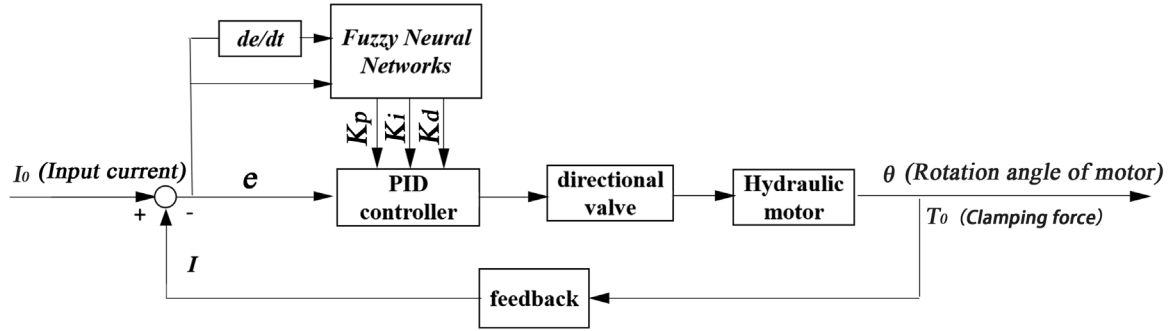


Fig. 6. Flow chart of PID control of fuzzy wavelet neural network.

FWNN as the fuzzy neural network for PID control. The FWNN designed in this paper is divided into 6 layers, which are input layer, fuzzification layer, fuzzy inference layer, wavelet layer, wavelet product layer, and output layer. Its structure is listed in the Figure 7.

1) Input layer. The input layer uses two neuron nodes, representing the deviation  $e$  and the deviation change rate  $de/dt$  of the control system. Its input activation function is  $f_1(x_i) = x_i$ .

2) Fuzzification layer. The role of this layer is to fuzzify the two inputs. Take and the fuzzy subset of deviation  $e$  and deviation change rate  $de/dt$  as {NB, NM, NS, ZO, PS, PM, PB}, namely {negative big, negative medium, negative small, zero, positive small, positive medium, positive big}, a total of 7 neuron nodes. The designed fuzzy neural network PID controller adopts incremental PID control. The fuzzy neural network is used to locally fine-tune the three parameters of  $K_p$ ,  $K_i$  and  $K_d$  on the basis of determining the basic range of PID controller parameters. Therefore, the range of the fuzzy set can be set to be very small. In this paper, the value range of the fuzzy set is set to  $[-6, 6]$  according to the reference [22]. Its input can be expressed as:

$$r_{ij} = x_i + \mu_{ijn-1} \alpha_{ij}$$

where:

$n$  — number of iterations

$\alpha_{ij}$  — weight of recursive feedback connection

$\mu_{ijn-1}$  — Gaussian membership function.

The output signal of the second layer is:

$$f_2(i, j) = \exp\left(-\frac{(r_i - c_{ij})^2}{(b_j)^2}\right)$$

In the formula:  $i=1, 2; j=1, 2, \dots, n; c_{ij}$  and  $b_j$  represent the center value and width value of the membership function, respectively.

3) Fuzzy inference layer. The main function of this layer is to perform fuzzy reasoning according to the set fuzzy rule table to determine the changing trend of PID parameters. This layer completes the matching of fuzzy rules through the connection with the fuzzification layer, and performs fuzzy operations between nodes. The calculation formula

used in this layer is:

$$f_3(j) = \prod_{i=1}^N \mu_{ij}(f_2(i, j))$$

where:

$$N = \prod_{i=1}^n n_i \text{ — sum of neurons}$$

4) Wavelet layer. Each input signal  $f_3(j)$  from layer 3 is passed through the activation function of the wavelet node. The activation function is:

$$f_4(j) = \left(1 - \frac{\|f_3(j) - t_j\|^2}{d_j^2}\right) \exp\left(-\frac{\|f_3(j) - t_j\|^2}{2d_j^2}\right)$$

where:

$d_j$  — scaling parameters of wavelet nodes

$t_j$  — translation parameters for wavelet nodes

$w_j$  — weight of the  $j$ th node of neural network

5) Wavelet product layer. This layer is similar to the third layer of fuzzy inference, which completes the matching of fuzzy rules through the connection with the wavelet layer and performs fuzzy operations between nodes. The main purpose of designing this layer is to perform fuzzy reasoning on the results after waveletization to determine a more precise adjustment range of PID parameters. The calculation formula used in this layer is:

$$f_5(j) = \prod_{i=1}^N (f_4(j))$$

where:

$$N = \prod_{i=1}^n n_i \text{ — sum of neurons}$$

6) Output layer. The role of this layer is to output the three control parameters of the PID controller. Its calculation formula is:

$$f_6(i) = w \cdot f_5 = \sum_{j=1}^N w(i, j) \cdot f_5(j)$$

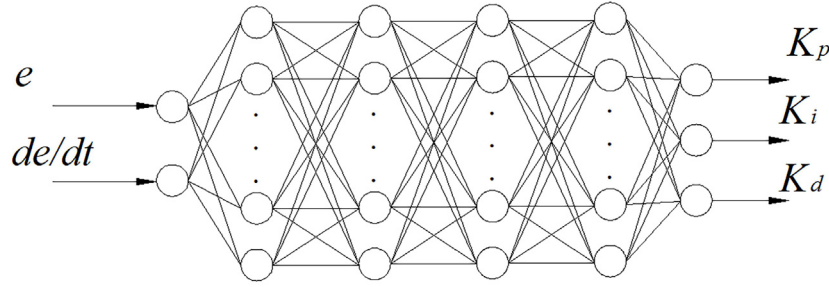


Fig. 7. Structure of the fuzzy wavelet neural network.

which is:

$$K_P = \sum_{j=1}^N w(1, j) \cdot f_5(j)$$

$$K_i = \sum_{j=1}^N w(2, j) \cdot f_5(j)$$

$$K_d = \sum_{j=1}^N w(3, j) \cdot f_5(j)$$

where:

Among them,  $w$  is the connection weight matrix between the fuzzy inference layer and the output layer.

The traditional FWNN neural network uses gradient descent method for training, but the disadvantage of this training method is that the training speed is slow with huge training samples, which cannot meet the real-time requirements of Camellia fruit picking. Therefore, the training methods of neural network need to be optimized by the modern optimization methods.

## 4 Improved learning algorithm of GWO-optimized neural network

### 4.1 Introduction to hybrid learning algorithms

The learning process of the traditional fuzzy wavelet neural network (FWNN) is to obtain the optimal weights and parameters by continuously adjusting the network parameters. However, the initial value of the traditional neural network parameters is random, which makes the network optimization easy to fall into the local minimum value, and the convergence is slow. The Grey Wolf Optimization Algorithm is a swarm intelligent optimization algorithm with strong global search ability, which is beneficial for accelerating the speed of neural network learning process and compensating for the problem of slow training speed caused by simply using gradient descent method. Therefore, this paper proposes to train the parameters  $d_{ij}$ ,  $t_j$  and  $w$  of the neural network by using the method of mixing the improved grey wolf optimizer and the gradient descent method. The approximate optimal solution of the network

weight parameters is obtained by improving the global search ability of the GWO, and then the gradient descent method is used to adjust the accuracy.

### 4.2 Gradient descent method

The gradient descent method is used to adjust the parameters of the neural network to determine the network weights. The performance indicators of the neural network are selected as:

$$E = \frac{1}{2} [e(k)]^2 = \frac{1}{2} [r(k) - y(k)]^2 \quad (19)$$

After determining the objective cost function, the network performs back-propagation, and performs gradient descent search with the goal of minimizing the objective function. In the search process, the iterative formula of each network parameter is:

$$\begin{cases} d_{ij}(k) = d_{ij}(k-1) + \Delta d_{ij}(k) + \alpha [d_{ij}(k-1) - d_{ij}(k-2)] \\ t_j(k) = t_j(k-1) + \Delta t_j(k) + \alpha [t_j(k-1) - t_j(k-2)] \\ w(k) = w(k-1) + \Delta w(k) + \alpha [w(k-1) - w(k-2)] \\ \Delta d_{ij} = -\eta \frac{\partial E}{\partial d_{ij}} \\ \Delta t_j = -\eta \frac{\partial E}{\partial t_j} \\ \Delta w(k) = -\eta \frac{\partial E}{\partial w} \end{cases} \quad (20)$$

where:

- $\eta$  — the learning rate;
- $\alpha$  — the momentum factor.

### 4.3 Improved grey wolf optimizer

#### 4.3.1 Introduction to grey wolf optimization algorithm

The grey wolf optimization algorithm simulates the strict social division of labor and cooperative hunting mode of grey wolves under natural environmental conditions, thereby realizing the determination of the optimal solution [24,25]. As grey wolves round up their prey, their hunting behavior is defined as follows:

$$D = |C \cdot X_p(t) - X(t)|$$



$$X(t+1) = X_p(t) - A \cdot D$$

where:

$D$  — the distance between individual wolves and their prey;

$X_p(t)$  — the position of the  $t$ th generation of prey;

$X(t)$  — the position of the individual in the  $t$ th generation of wolves;

$A$  &  $C$  — the coefficients, its calculation formula is shown in formulas (21) and (22):

$$A = 2a \cdot r_1 - a \quad (21)$$

$$C = 2r_2 \quad (22)$$

Among them:  $a$  is the convergence factor, which decreases linearly from 2 to 0 with the number of iterations;  $r_1$  and  $r_2$  are random numbers between 0 and 1.

The grey wolf's social hierarchy is a 4-tier pyramid structure. The  $\alpha$ -wolf is located at the top of the pyramid, which is the supreme leader of the wolf pack and is responsible for the planning and decision-making of the overall hunting. The  $\beta$ -wolf is located on the second layer of the pyramid and is mainly responsible for assisting the  $\alpha$ -wolf in decision-making. When the  $\alpha$ -wolf is vacant, the  $\beta$ -wolf will replace the  $\alpha$ -wolf as the leader. The  $\delta$ -wolf is located on the third layer of the pyramid. It obeys the decision-making orders of the  $\alpha$ -wolf and the  $\beta$ -wolf, and is mainly responsible for tasks such as reconnaissance, sentry, and care babies. The  $\omega$ -wolves are located at the bottom of the pyramid and play a role in balancing relationships within the population.

The  $\alpha$ -wolf,  $\beta$ -wolf and  $\delta$ -wolf are the wolves that are closest to and most aware of the presence of their prey when encircling their prey. The  $\beta$ -wolf and  $\delta$ -wolf led by alpha wolf, will lead the entire pack to surround their prey. Its mathematical expression is as follows:

$$\begin{cases} D_\alpha(t) = |C_1 X_\alpha(t) - X(t)| \\ D_\beta(t) = |C_2 X_\beta(t) - X(t)| \\ D_\delta(t) = |C_3 X_\delta(t) - X(t)| \end{cases} \quad (23)$$

$$\begin{cases} X_1(t) = X_\alpha(t) - A_1 D_\alpha(t) \\ X_2(t) = X_\beta(t) - A_2 D_\beta(t) \\ X_3(t) = X_\delta(t) - A_3 D_\delta(t) \\ X(t+1) = \frac{X_1(t) + X_2(t) + X_3(t)}{3} \end{cases} \quad (24)$$

where:

$D_\alpha(t)$  — the distance between the  $t$ th generation of wolves and  $\alpha$ -wolf individuals;

$D_\beta(t)$  — the distance between the  $t$ th generation of gray wolf individuals and  $\beta$ -wolf individuals;

$D_\delta(t)$  — the  $t$ th generation. distance between individual wolf packs and  $\delta$ -wolf individual;

Equation (24) defines the step size and direction of the individual  $\omega$ -wolf in the wolf pack toward the  $\alpha$ -wolf, the  $\beta$ -wolf and the  $\delta$ -wolf, and the final position of the new generation of grey wolves.

### 4.3.2 Improved grey wolf optimization algorithm

The ultimate goal of the algorithm in this paper is to minimize the deviation value. Therefore, the time multiplied absolute value error integration criterion ITAE index is selected as the fitness function  $J$  of the GWO algorithm. The calculation formula is:

$$J = \int_0^N t \cdot |e(t)| dt \quad (25)$$

where:

$N$  — the total number of iteration steps of the gray wolf algorithm;

It has the problem of slow convergence and easy formation of local optimum, since the traditional GWO algorithm ignores the information exchange between the grey wolf and its own experience. Therefore, the improvement of the convergence factor  $a$  and the control parameter  $C$  is as follows:

$$a = \left[ 2 - \frac{2t}{t_{\max}}, \frac{1}{1 + \exp((t - 0.25t_{\max})/(0.025t_{\max}))} \right] \quad (26)$$

$$\begin{cases} C_1 = 2r_2 - A \\ C_2 = 2r_2 + A \end{cases} \quad (27)$$

In the formula,  $a, C_1, C_2 \in [2, 0]$ ,  $t = 1, 2, \dots, t_{\max}/2$

$t_{\max}$  — the maximum number of iterations;

That is to say, from the beginning of the iteration to half of the maximum number of iterations, the convergence factor  $a$  decreases linearly from 2 to 0. The  $\alpha$ -wolf and the  $\beta$ -wolf achieve positional alternation in the subsequent iteration cycle, and the  $\beta$ -wolf with better physical strength leads the wolf group to approach the prey until the prey is captured [26].

### 4.3.3 Hybrid algorithm to optimize neural network

The designed algorithm is denoted as the IGWO-FWNN-PID algorithm, and its specific working process is as follows:

Step 1: Build the fuzzy neural network PID control model, determine the network topology, and initialize the fuzzy neural network parameters  $d_{ij}$ ,  $t_j$  and  $w$ .

Step 2: Initialize wolf pack size, individual location, number of iterations, and values of  $a$ ,  $A$ , and  $C$ .

Step 3: Calculate the distance between the individual grey wolves and the prey using formula (23), and set the top three wolves with the shortest distance from the individual to the prey as  $\alpha$ -wolf,  $\beta$ -wolf and  $\delta$ -wolf.

Step 4: Surround the prey, and update the individual position of the wolf pack using formula (24), where  $w$  takes its initial value  $w_0$  in the first update.

Step 5: Update the values of  $a$ ,  $A$ , and  $C$  are updated using equations (21), (26), and (27).

Step 6: Calculate the distance between the new generation of wolves and the prey, and update the  $\alpha$ -wolf,  $\beta$ -wolf and  $\delta$ -wolf according to the results.

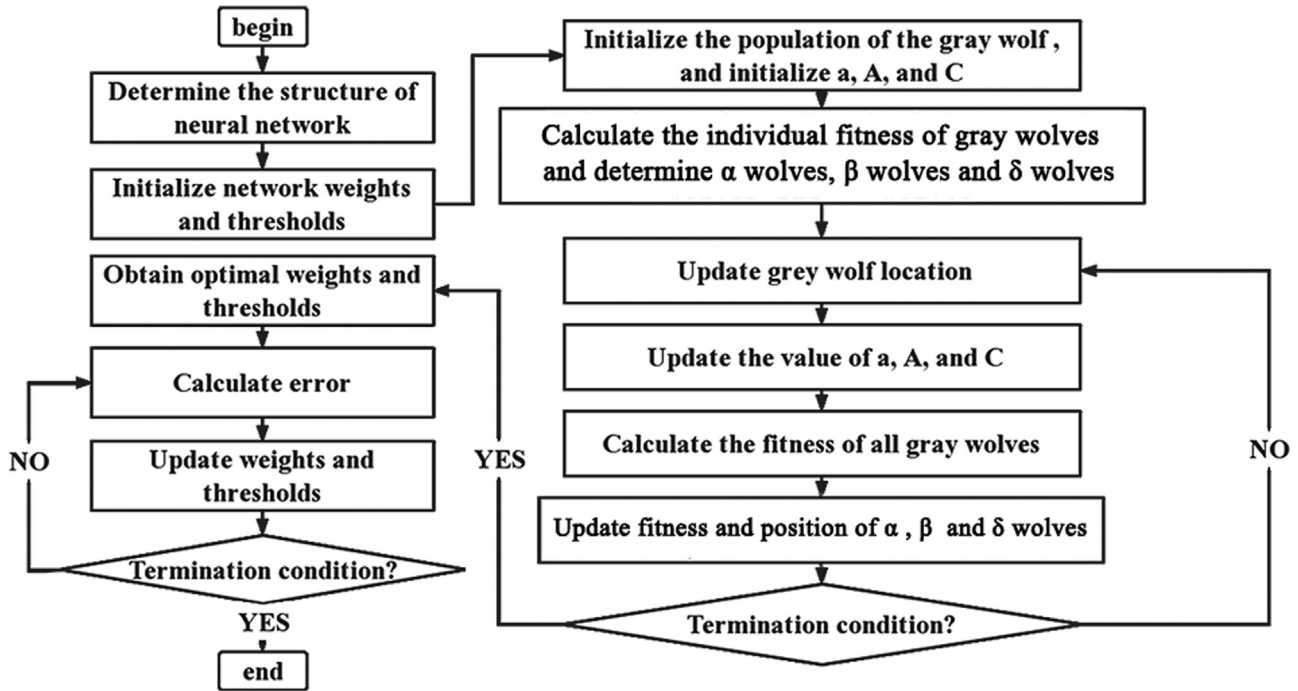


Fig. 8. Flowchart of hybrid algorithm optimization.

Step 7: Determine whether the maximum number of iterations is reached. If YES, output the optimization result to the fuzzy neural network, and go to the next step. If NO, return to step 4.

Step 8: After the fuzzy neural network obtains the initial value of the parameters, forward propagation is performed, and the deviation is calculated according to the formula (19). Then use the gradient descent method for back-propagation, update the network parameters online according to formula (20), and finally output the optimal  $K_P$ ,  $K_I$ ,  $K_D$ .

The flow chart of the above algorithm is present in Figure 8.

## 5 MATLAB/Simulink simulation and experimental analysis

### 5.1 MATLAB/Simulink simulation

In order to verify the effect of the IFWNNPID controller designed in this paper, the simulation experiment was carried out in Simulink. The controller simulation module is shown in Figure 9. The simulation running environment is in Windows 10 64-bit operating system with MATLAB R2018a software platform, and the simulation computer CPU is Intel Core i5-9400F of which the main frequency is 2.9 GHz and the memory is 16GB. The simulation time was set in 10s. The parameters used in the simulation are listed in Table 1 and shown in Table 2.

The step signal was selected as the input of the simulation in the experiment, and traditional PID controller, fuzzy PID controller and FWNN PID controller were added for comparison in order to verify the effect of the controller designed in this paper.

A step signal with 550 mA at 0s was input to the whole system in the case of ideal and no interference. It obtained the step response curve obtained by the simulation as presented in Figure 10.

As can be seen from Figure 10, the clamping force of the PID controller is maintained at about 315.15 N after 3.515 s, while the FPID controller keeps the clamping force at about 307.72 N after 3.236 s. The FWNN PID controller preserves clamping force in 304.32 N after 3.082 s, while the IFWNN PID controller maintains the clamping force at about 303.15 N after 3.027 s. It can be seen that the response of the PID controller and the FPID controller is relatively slow, and the clamping force is maintained at a relatively large level, while the response speed of the FWNNPID controller is faster than the previous two controllers, and the output value of the clamping force is relatively good.

A white noise signal as shown in Figure 11 is applied to the output clamping force of the actuator to simulate the interference effect of the environment on the clamping jaws in order to verify the performance of the IFWNN PID controller under the condition of external interference. The response curve of the system obtained from the simulation is shown in Figure 12. The input current change curve and error response curve of the IFWNN PID control system are presented in Figures 13 and 14. The output shaft torque  $T_0$  and the output angle  $\theta$  of the clamping hydraulic motor are listed in Figures 15 and 16.

It can be seen from Figure 12 that both the PID and FPID controllers produce large fluctuations in the clamping force when the end of the gripper is disturbed, while the FWNN PID controller and the IFWNN PID controller produce relatively small fluctuations in the clamping force, which means that the fuzzy neural network PID controller has better robustness than PID and FPID controllers, and

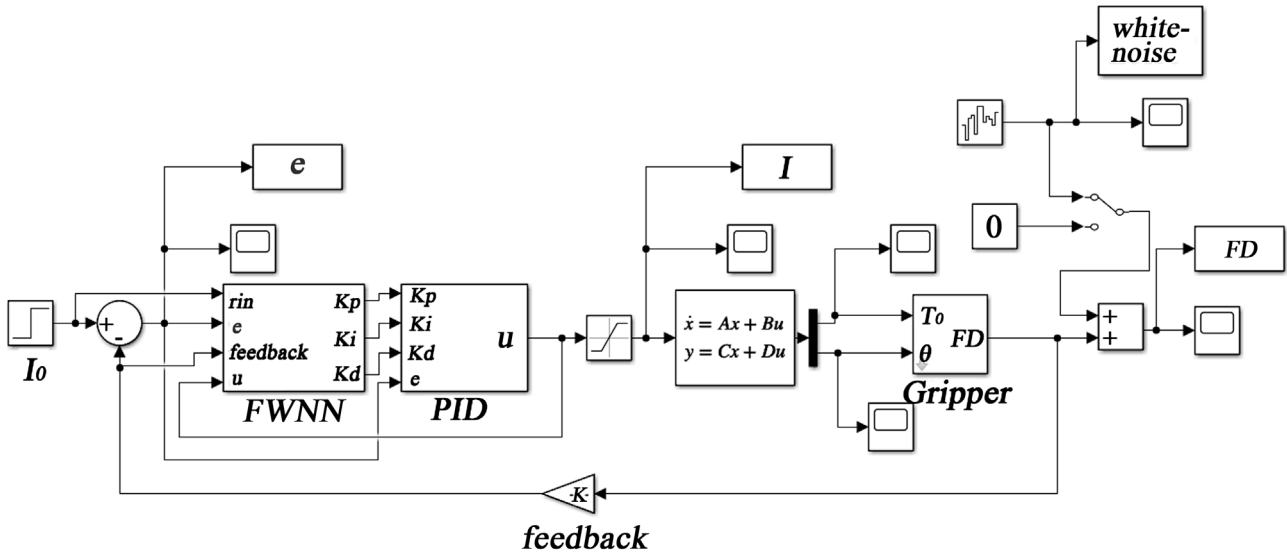


Fig. 9. Simulation model of FWNNPID controller.

Table 1. The table of the simulation parameter.

Electro-hydraulic proportional direction valve		Hydraulic motor		Clamping jaws	
$k_i$	$8 \text{ mm} \cdot (\text{mA})^{-1}$	$G$	$62 \text{ N} \cdot \text{mm} \cdot \text{deg}$	$l_{AB}$	$139 \text{ mm}$
$k_q$	$13.3 \text{ ml/mm}$	$J_t$	$1347.80 \text{ kg} \cdot \text{mm}^2$	$l_{BC}$	$50 \text{ mm}$
$k_c$	$0.027 \text{ ml} \cdot \text{s}^{-1} \cdot \text{MPa}$	$D$	$18.20 \text{ ml/r}$	$d_{CD}$	$100 \text{ mm}$
$E$	$0.7 \text{ GPa}$	$c_m$	$15 \text{ N} \cdot \text{mm/deg}$	$e$	$90 \text{ mm}$
		$V_m$	$18.77 \text{ ml}$	$i$	$2$
		$K_{cm}$	$1.2$	$L$	$10 \text{ mm}$
				$\eta_1$	$0.95$
				$\eta_2$	$0.88$

Table 2. Parameters of the fuzzy wavelet neural network.

$\eta$	$\alpha$	$a$	$C_1$	$C_2$
0.2	0.05	2	2	2

can maintain the clamping force within a range of relatively stable values. It can be seen that when the system starts the clamping operation function, the electromagnet of the electro-hydraulic proportional direction valve is energized, the valve core moves to make the hydraulic oil enter the hydraulic motor, and the output shaft torque of the hydraulic motor rises rapidly combining with Figures 13–16. At this time, the clamping force of the gripper increases rapidly, and the adjustment error of the neural network decreases rapidly. After 3.027 s, the system reaches the set clamping force value, the current of the electromagnet decreases rapidly, the opening of the valve port decreases, and the torque of the output shaft of the clamping hydraulic motor decreases. When disturbed by external interference signals, the control system mainly adjusts the

input small current to realize the flexible adjustment of the valve opening of the electro-hydraulic proportional direction valve, which can adjust the output angle of the hydraulic motor, so as to realize the control of the output of the clamping hydraulic motor that keeps the clamping force as a constant. The stronger the white noise signal the gripper receives, the more severe the input current changes, and the greater the output angle adjustment value.

In summary, the FWNNPID controller has the advantages of faster response speed, relatively stable clamping force and better robustness compared with the general PID controller and fuzzy PID controller under the condition of no interference and external white noise interference at the end of the gripper. This means that the controller can not only ensure the stable clamping of the camellia trunk during

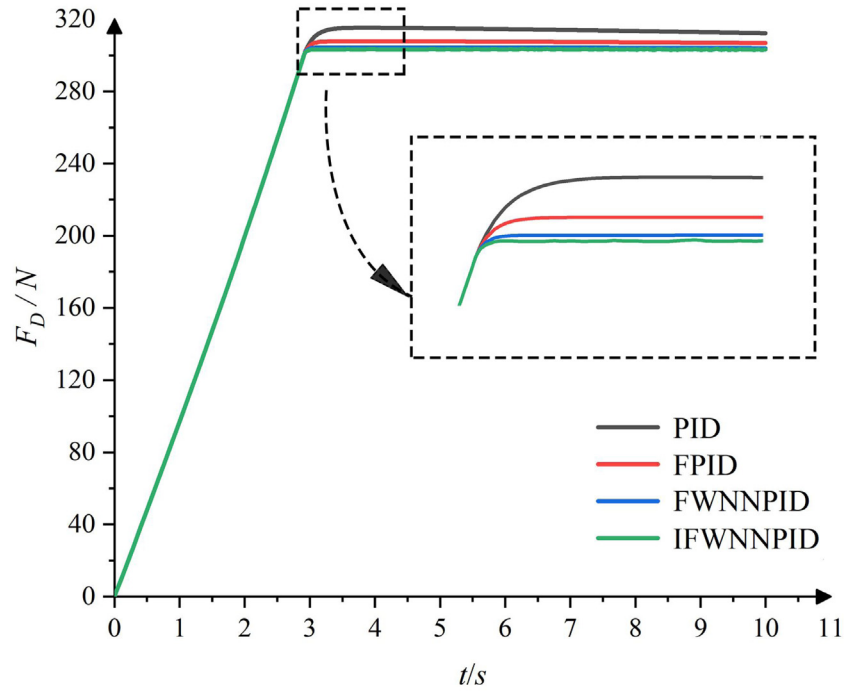


Fig. 10. Response without disturbance.

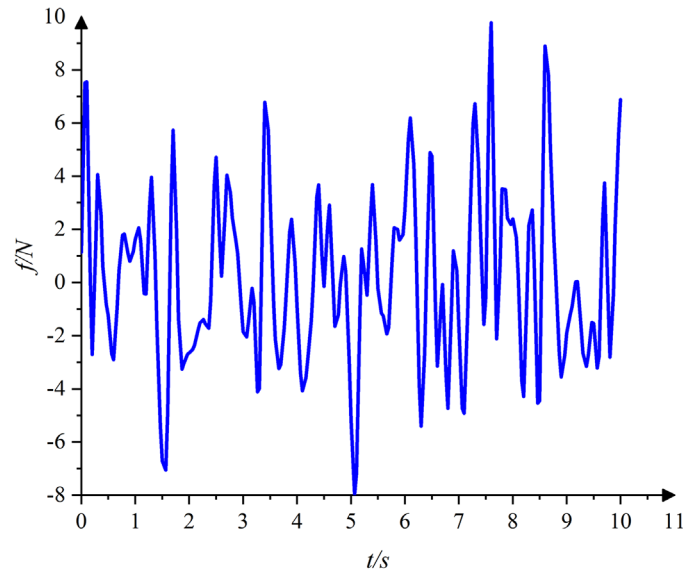


Fig. 11. Input white noise signal.

vibration operation, but also avoids damage to the camellia trunk caused by excessive clamping force.

## 5.2 Field test of the manipulator

In order to verify the control effect of the designed picking manipulator, our research team conducted a camellia fruit field test on October 18, 2021 at the experimental base of Xuefengshan Camellia Society in Wangcheng District, Changsha City, Hunan Province, China. The test time was

9:30 am, the weather was cloudy, the temperature was 15°C, and the air humidity was 86%. The designed test prototype is shown in Figure 17. The prototype adopts IFWNNPID controller and traditional PID controller respectively for picking test.

Picker control system consists of single board computer, driver, motion controller and sensor. The control system of the prototype consists of a single-board computer, a driver, motion controllers and sensors. The upper computer adopts the single-board computer EasyDL-JetsonNano,

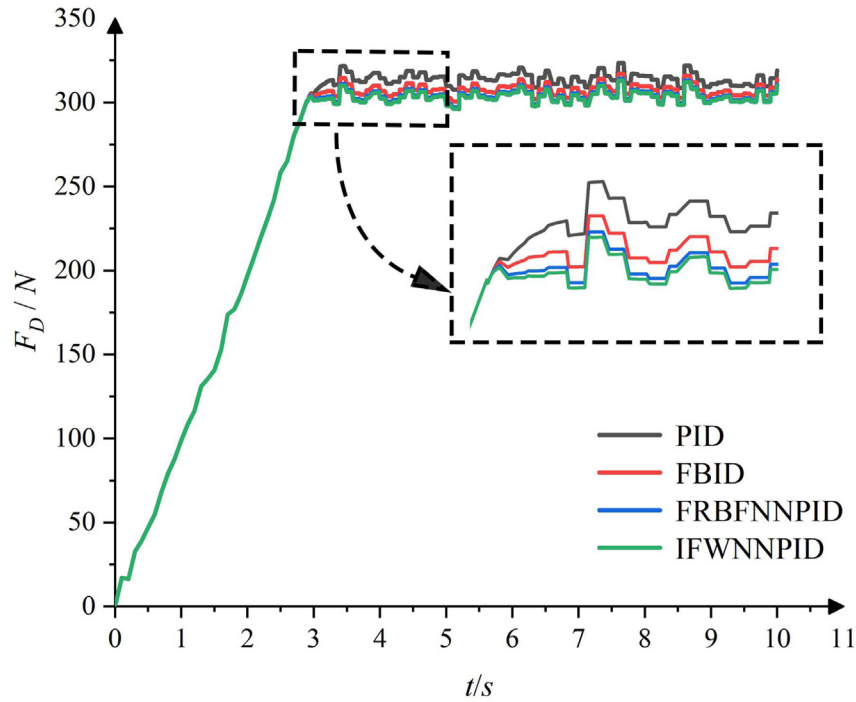


Fig. 12. Response in the presence of interference.

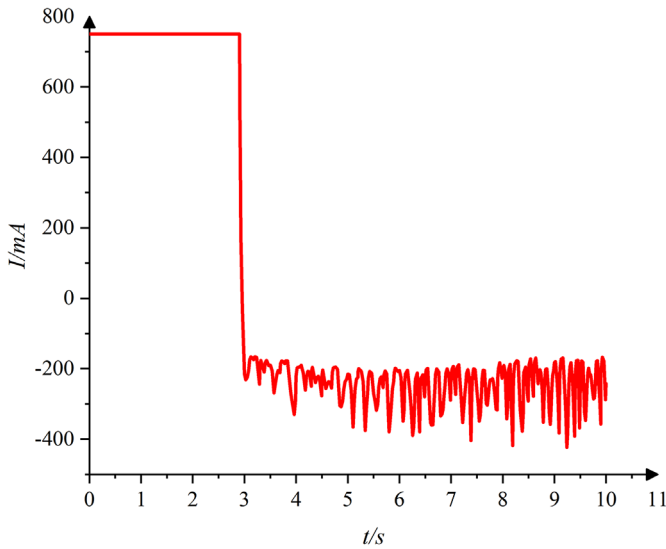


Fig. 13. Response curve of the input current.

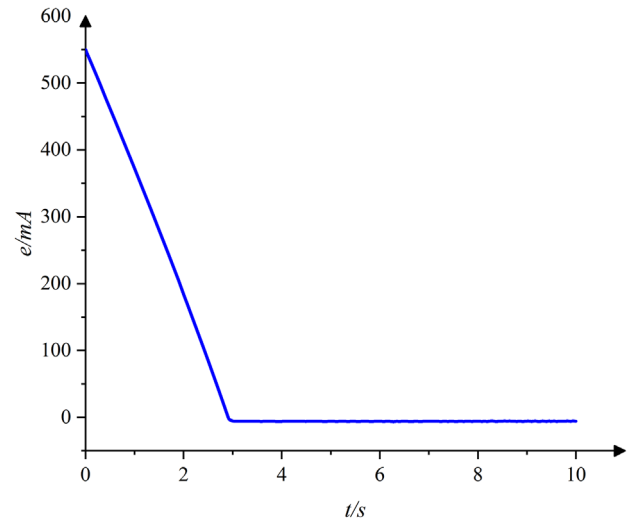


Fig. 14. Error curve of the neural network.

which is mainly used for receiving sensor signals, image processing and motion position calculation, while the lower computer adopts the single-chip STM32F405RGT6 as the controller of the actuator. The MP3V5004DP-SMD-8 pressure sensor is installed on the side of the manipulator clamping jaws to detect the clamping force of the manipulator.

The prototype of camellia fruit picking machine first determined a camellia tree to be picked through its vision system (Monocular camera with FUJINON HF16SA-1&binocular CMOS camera), and transmitted the data of the tree to the Jetson Nano. The Jetson Nano

automatically planned the movement trajectory of the picking manipulator according to the transmitted data, and calculated the joint angles driven by the hydraulic actuator required for each movement. Then it transmitted the signal to the lower computer to drive the picking manipulator to move and grip the target camellia tree. When the manipulator moved to the designated position, the control system controlled the electro-hydraulic proportional direction valve to work and clamped the hydraulic motor to grip the camellia trunk. And then the control system started the vibration picking function after the clamping operation was completed.

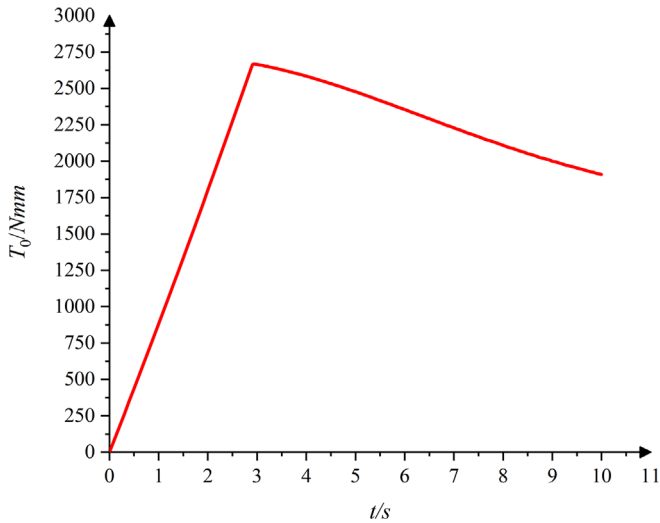


Fig. 15. Output shaft torque curve of clamping hydraulic motor.



Fig. 17. Push-and-shaking camellia fruit picking machine.

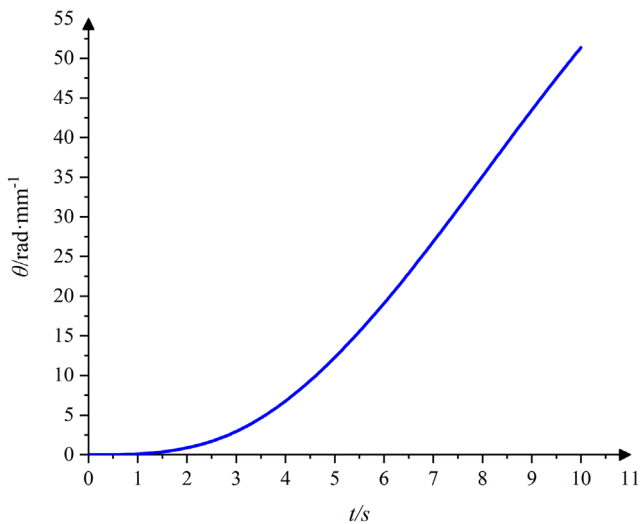


Fig. 16. Change curve of output angle of clamping hydraulic motor.

In this test, 9 groups of camellia trees were designed to be clamped. The clamping height of branches with similar diameters was 1000 mm, and the clamping was repeated 3 times for each group of camellia trees. The trunk diameter was measured with a meter ruler, the clamping movement time was counted with a stopwatch, the maximum clamping force was recorded by a pressure sensor, and the clamping damage length was measured with a scale. The picker was started vibrate picking, and visually observed whether the clamping is loose after stable clamping. The test results show that under the action of the two controllers mentioned above, there is no phenomenon that the clamping jaws loosen the camellia tree during the vibration picking. Figures 18

and 19 show the effect of clamping damage left after the picking test, and the measured test data are presented in Tables 3 and 4.

It can be seen that IFWNN PID controller to drive the gripper clamping operation compared with the PID controller shorted the clamping time in 20.0 % and reduced the clamping damage in 13.6% from Figure 18 and the data comparison between Tables 3 and 4. The above results show that the designed IFWNN PID controller can effectively control the damage of camellia branches caused by excessive clamping force, and can meet the clamping force requirements of the camellia fruit picking machine. However, it can also be seen from the above test results that there is still room for optimization in the mechanical structure of the above-mentioned camellia fruit picker, and the clamping force damage can be further reduced by improving the structure of the clamping jaw.

## 6 Conclusion

The state space equation of the valve-controlled clamping hydraulic motor system of the push-and-shaking camellia fruit picking manipulator was deduced, and the control system was designed based on FWNN PID controller optimized by improved GWO algorithm aiming at the problem that the constant clamping force of the mechanical jaws of the push-and-shaking camellia fruit picking manipulator reduces the damage of the holding tree trunk. Finally, MATLAB/Simulink software was used for simulation analysis under no interference and interference situations and a field test was carried out. The results show that the manipulator controlled by the IFWNN PID controller can effectively reduce the clamping movement time, reduce the damage of the clamping force, and has

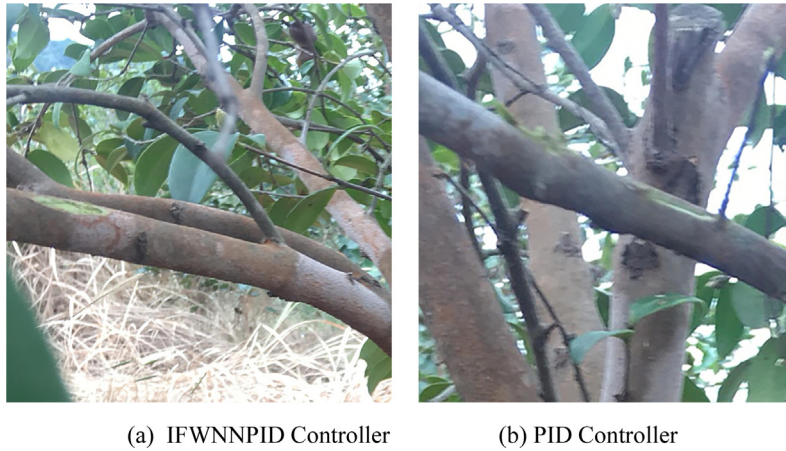


**Fig. 18.** Damage of clamping tree trunk compared with PID controller and IFWNN PID controller.

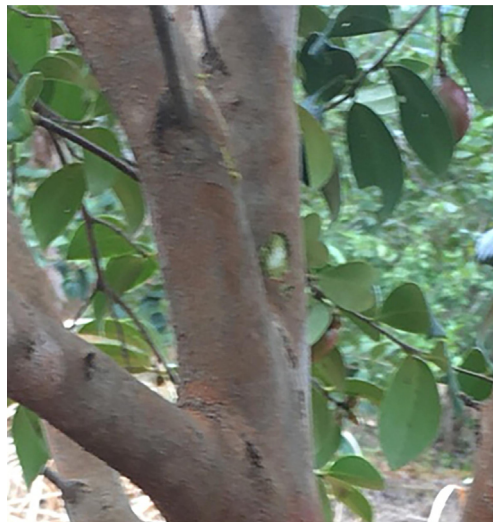


**Fig. 19.** Damage of trunk clamped under the IFNNPID controller.

**Table 3.** Analysis of the clamping force with the PID controller.

Test group	Average diameter of trunk (mm)	Clamping movement time (s)	Maximum clamping force (N)	Clamping damage length (cm)
1	45.6	3.42	659	55.2
2	44.8	3.57	627	51.6
3	48.2	3.76	694	52.6
4	53.4	4.26	786	47.9
5	52.8	4.59	825	48.9
6	55.4	4.36	843	42.7
7	58.7	4.97	962	24.6
8	60.3	4.86	1069	33.4
9	62.7	4.92	1012	25.4
Average		4.30	830.78	42.48

**Table 4.** Analysis of the clamping force with the IWNNPID controller.

Test group	Average diameter of trunk (mm)	Clamping movement time (s)	Maximum clamping force (N)	Clamping damage length (cm)
1	45.6	3.12	624	47.2
2	44.8	3.14	589	46.8
3	48.2	3.26	556	42.7
4	53.4	3.34	723	40.5
5	52.8	3.36	789	43.1
6	55.4	3.58	754	38.2
7	58.7	3.84	846	21.4
8	60.3	3.68	896	23.7
9	62.7	3.62	837	26.8
Average		3.44	734.89	36.71

better robustness, which can satisfy the clamping operation requirements of the push-and-shaking camellia fruit picking mechanical manipulator.

### Funding information

This project was supported by the Key Research and Development Program of Hunan Province of China under Grant 2021NK2023 and Postgraduate Science and Technology Innovation Fund Project of Central South University of Forestry and Technology (CX202102038).

### Conflicts of Interest

The authors have no conflict to disclose.

### References

- [1] W. Wang et al., Active role of tea oil in medicine and health care, *Food Nutr. China* 48–51 (2007)
- [2] Z. Gao et al., Development and experiment of the picking actuator of the comb-type camellia fruit picking machine, *Trans. Chin. Soc. Agric. Eng.* **29**, 19–25 (2013)
- [3] D. Huang, H. Rao, Research present situation of mechanized picking equipment for Camellia in China, *For. Mach. Woodwork. Equip.* **47**, 11–13 (2019)
- [4] L. Zhang et al., Design and experiment of mechanical picking platform of Camellia based on Matlab, *China South. Agric. Mach.* **48**, 22–24 (2017)
- [5] D. Wu et al., Research progress and trend of camellia fruit picking equipment in China, *J. Chin. Agric. Mech.* **43**, 186–194 (2022)
- [6] Z. Gao et al., Design and test of suspension vibrating Camellia picking executing mechanism, *Trans. Chin. Soc. Agric. Eng.* **35**, 9–17 (2019)
- [7] W. Qing, A. Li, Y. Li, J. Liu, H. Shen, G. Li, Microtension control for a yarn winding system with an IMC PID controller, *Mech. Ind.* **20** (2019)
- [8] R.J. Mozhddehi, A.S. Ghafari, Optimal PID control of a nano-Newton CMOS-MEMS capacitive force sensor for biomedical applications, *Mech. Ind.* **15**, 139–145 (2014)
- [9] K.K. Ayten, M. Hüseyin Çiplak, A. Dumlu, Implementation a fractional-order adaptive model-based PID-type sliding mode speed control for wheeled mobile robot *Proc. Inst. Mech. Eng. I: J. Syst. Control Eng.* **233**, 1067–1084 (2019)
- [10] M.S. Ayas, I.H. Altas, Designing and implementing a plug-in type repetitive controller for a redundantly actuated ankle rehabilitation robot, *Proc. Inst. Mech. Eng. I: J. Syst. Control Eng.* **232**, 592–607 (2018)
- [11] B. Lin, X. Su, X. Li, Fuzzy sliding mode control for active suspension system with proportional differential sliding mode observer, *Asian J. Control* **21**, 264–276 (2019)
- [12] L. Kong, J. Yuan, New relaxed stabilization conditions for discrete-time Takagi-Sugeno fuzzy control systems, *Asian J. Control* **22**, 1604–1616 (2020)
- [13] Z. Wang, Y.S. Huang, Robust decentralized adaptive fuzzy control of large-scale nonaffine nonlinear systems with strong interconnection and application to automated highway systems, *Asian J. Control* **21**, 2387–2394 (2019)
- [14] D. Tufan, C.M. Serhat, Design and robustness analysis of fuzzy PID controller for automatic voltage regulator system using genetic algorithm, *Trans. Inst. Meas. Control* **44**, 1862–1873 (2022)
- [15] S. Han, J.F. Dong, J. Zhou, Y.H. Chen, Adaptive fuzzy PID control strategy for vehicle active suspension based on road evaluation, *Electronics* **11**, 921–921 (2022)
- [16] J. Xu, L. Xiao, M. Lin, X. Tan, Application of fuzzy PID position control algorithm in motion control system design of palletizing robot, *Secur. Commun. Netw.* (2022)
- [17] F. Xue, Z. Fan, Kinematic control of a cable-driven snake-like manipulator for deep-water based on fuzzy PID controller, *Proc. Inst. Mech. Eng. I: J. Syst. Control Eng.* **236**, 989–998 (2022)
- [18] Q. Wu, Y. Zhang, Y. Chen, Design, control, and experimental verification of a soft knee exoskeleton for rehabilitation during walking, *Proc. Inst. Mech. Eng. I: J. Syst. Control Eng.* **236**, 138–152 (2022)
- [19] H.L. Guo, K.W. Li, Research on control system for sluice gate flow based on fuzzy neural network PID, *Appl. Mech. Mater.* **1945**, 1779–1782 (2012)
- [20] Z.C. Zhou, R. Chen, Design on fuzzy neural network PID control system of diesel engine, *Adv. Mater. Res.* **2534**, 425–429 (2013)



- [21] C. Gong, S. Yang, Research of oil pump control based on fuzzy neural network PID algorithm, *Int. J. Adv. Netw. Monitor. Controls* **3**, 63–68 (2019)
- [22] J.J. Xu, L. Xiao, M. Lin, X. Tan, Application of fuzzy PID position control algorithm in motion control system design of palletizing robot, *Secur. Commun. Netw.* (2022)
- [23] Z. Gao et al., The design and analysis of Camellia fruit picking robots' picking monomers, *J. Central South Univ. For. Technol.* **36**, 114–118 (2016)
- [24] Z. Fan, L.J. Li, Y.H. Li et al., Trajectory planning of camellia fruit picking manipulator based on improved grey wolf optimization, *Mach. Des. Res.* **38**, 195–201 (2022)
- [25] S. Mirjalili, S. Mohammad Mirjalili, A. Lewis, Grey wolf optimizer, *Adv. Eng. Softw.* **64**, 46–61 (2014)
- [26] W. Liu, Z. Guo, F. Jiang, G. Liu, B. Jin, D. Wang, Improved grey wolf optimizer based on cooperative attack strategy and its PID parameter optimization, *J. Front. Comput. Sci. Technol.* **17**, 1–16 (2022)

**Cite this article as:** Z. Fan, L. Li, K. Liao, Z. Gao, Y. Li, H. Xie, Improved fuzzy neural network control for the clamping force of Camellia fruit picking manipulator, *Mechanics & Industry* **24**, 30 (2023)